BIOCHEMISTRY
including biophysical chemistry & molecular biology

Article

pubs.acs.org/biochemistry

Phycoviolobilin Formation and Spectral Tuning in the DXCF Cyanobacteriochrome Subfamily

Nathan C. Rockwell, Shelley S. Martin, Alexander G. Gulevich, and J. Clark Lagarias*

Department of Molecular and Cellular Biology, University of California, Davis, California 95616, United States

Supporting Information

ABSTRACT: Phytochromes are red/far-red photosensory proteins that regulate adaptive responses to light via photoswitching of cysteine-linked linear tetrapyrrole (bilin) chromophores. The related cyanobacteriochromes (CBCRs) extend the photosensory range of the phytochrome superfamily to shorter wavelengths of visible light. CBCRs and phytochromes share a conserved Cys residue required for bilin attachment. In one CBCR subfamily, often associated with a blue/green photocycle, a second Cys lies within a conserved Asp-Xaa-Cys-Phe (DXCF) motif and is essential for the blue/green photocycle. Such DXCF CBCRs use isomerization of the phycocyanobilin (PCB) chromophore into the related phycoviolobilin (PVB) to shorten the conjugated system for sensing green light. We here use recombinant expression of individual CBCR domains in *Escherichia coli* to survey the DXCF subfamily from the cyanobacterium *Nostoc punctiforme*. We describe ten new photoreceptors with well-resolved photocycles and three additional photoproteins with overlapping dark-adapted and photoproduct states. We show that the ability of this subfamily to form PVB or retain PCB provides a powerful mechanism for tuning the photoproduct absorbance, with blue-absorbing dark states leading to a broad range of photoproducts absorbing teal, green, yellow, or orange light. Moreover, we use a novel green/teal CBCR that lacks the blue-absorbing dark state to demonstrate that PVB formation requires the DXCF Cys residue. Our results demonstrate that this subfamily exhibits much more spectral diversity than had been previously appreciated.

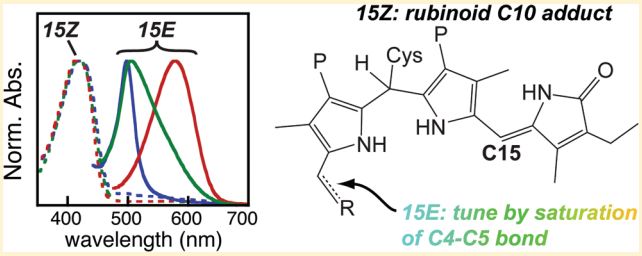

Photosynthetic organisms use a broad variety of photosensory systems to optimize their metabolism and light-harvesting apparatus.[1] Such sensors have historically been classed as mediators of blue-light responses or red-light responses. Blue-light responses often are mediated by proteins using flavin chromophores.[2−5] Red-light responses are instead mediated by phytochromes, which use linear tetrapyrrole (bilin) chromophores. Phytochromes function as critical regulators of photomorphogenesis in higher plants, as regulators of the light-harvesting apparatus in purple photosynthetic bacteria, and as regulators of fungal development and social responses in other systems.[6−11] Phytochromes photoswitch between red-absorbing (P_r) and far-red absorbing (P_{fr}) forms via photoisomerization about the 15,16-double bond of their covalently bound bilin chromophores.[9,12−14] The *15Z* configuration (P_r) is usually the dark state, and the *15E* configuration (P_{fr}) is usually a metastable photoproduct that can thermally decay to P_r via dark reversion.[13−17] All phytochromes share a photosensory core module comprising a GAF domain containing the bilin-binding pocket and a C-terminal PHY domain contacting the pocket via a conserved loop.[13−16,18−20]

Cyanobacterial phytochrome-related photosensors named cyanobacteriochromes (CBCRs) have been described more recently.[13,21−23] Phylogenetic analysis identifies several subfamilies of CBCRs.[22−25] Unlike phytochromes, CBCRs require only the isolated GAF domain for bilin attachment and for reversible photochemistry.[21,26] CBCRs and phytochromes from oxygenic photosynthetic organisms share a thioether linkage between the C3[1] atom of the bilin and a conserved Cys residue in the GAF domain (Figure S1A). Individual CBCR GAF domains do not exhibit the red/far-red[a] photocycles of conventional phytochromes; instead, they exhibit an astonishing diversity of photocycles, with examples ranging from the near-UV to the red region of the electromagnetic spectrum.[23−25,27−31] Cyanobacteria frequently contain multiple CBCRs arranged in tandem, and such proteins can even contain red/far-red phytochromes as well.[18,32,33] In this work, we define individual photosensory modules as CBCRs or phytochromes and thus consider tandem CBCRs or phytochrome/CBCR composites as larger, more complex sensors.

Multiple blue/green CBCRs already have been described, all of which share a second conserved Cys residue in the GAF domain as part of a larger Asp-Xaa-Cys-Phe (DXCF) motif.[21,24−27,31] Such DXCF CBCRs are found in genomes of a wide variety of cyanobacteria adapted to freshwater, marine, and soil environments. In some cyanobacterial species, such as *Thermosynechococcus elongatus*[22,24] and *Gloeobacter violaceus*,[34]

Received: December 2, 2011
Revised: January 26, 2012
Published: January 26, 2012

   dx.doi.org/10.1021/bi201783j | *Biochemistry* 2012, 51, 1449−1463

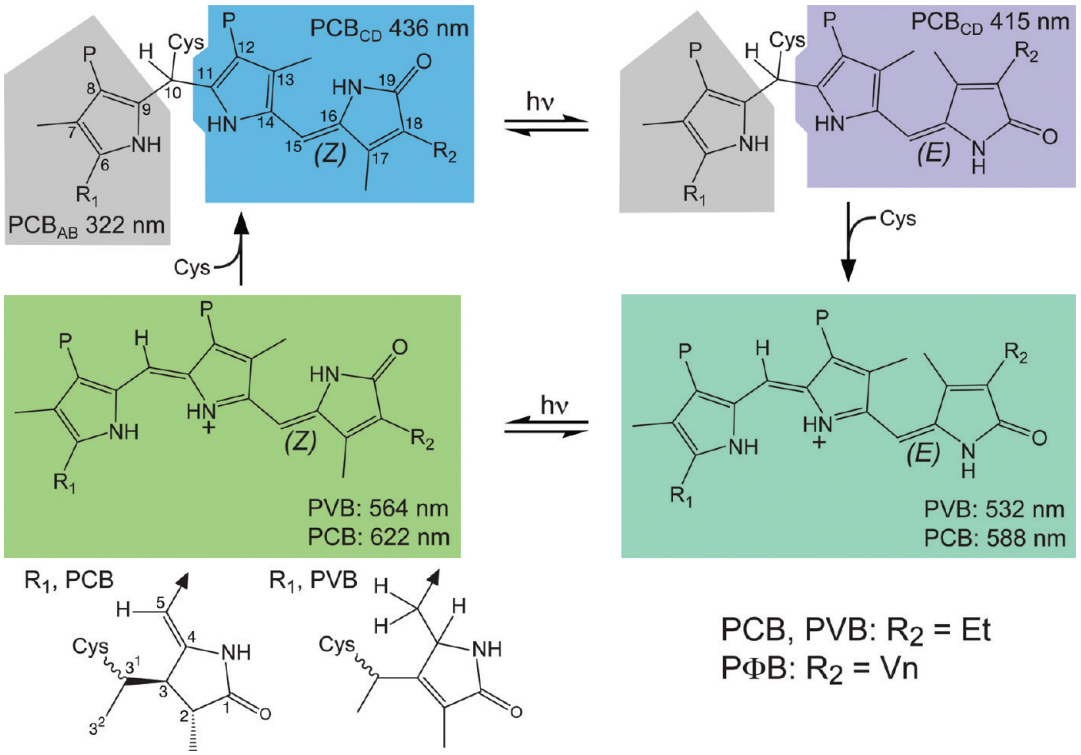

Figure 1. The two-Cys photocycle of blue/green DXCF CBCRs. In the blue-absorbing *15Z* dark state (left), there is a second covalent linkage between the C10 atom of the bilin chromophore and the "second" Cys residue of the DXCF motif. Photoconversion initially results in a *15E* photoproduct retaining this second linkage (top), with subsequent elimination of the Cys to restore conjugation across C10 and to red-shift the photoproduct absorbance (right). Photoconversion of this *15E* state results in a *15Z* species (bottom), which then regenerates the second linkage and completes the cycle. This cycle can utilize either PVB or PCB chromophores,[35] differing at C5 and in the A-ring (bottom left). Peak wavelengths are provided for Tlr0924 (ref 24 and this work). Species with an intact second linkage have two chromophoric systems centered on the C- and D-rings (PCB$_{CD}$) and on the A- and B-rings (PCB$_{AB}$). Et, ethyl; P, propionate; Vn, vinyl.

DXCF CBCRs are the only members of the phytochrome superfamily. The proliferation of the DXCF CBCR family in cyanobacteria underscores the importance of light sensing across the entire spectrum that can be harvested for photosynthesis.

Formation of the blue-absorbing dark state in DXCF CBCRs requires the DXCF Cys residue.[24,25,31,35] Such dual-Cys photocycles have also evolved independently in a second subfamily of CBCRs (the insert-Cys subfamily) and even in a variant phytochrome.[23] For all of these cases, we envisage that the second Cys forms a thioether linkage to the C10 atom of the bilin chromophore in the *15Z* dark state (Figure 1), conferring absorbance of near-UV, violet, or blue light.[23,24] This model is consistent with the known properties of bilin chromophores; in particular, it is known that the C10 atom can react with thiol compounds or other nucleophiles.[36−39]

Previously, four CBCRs have been characterized using both cyanobacterial expression and recombinant expression in *E. coli* engineered to produce bilin chromophores.[29,31,35,40] All four accept phycocyanobilin (PCB) as the chromophore precursor, forming a PCB adduct after covalent attachment of the first Cys. Unlike other CBCRs, DXCF CBCRs can autocatalytically isomerize initially formed PCB adducts into phycoviolobilin (PVB) adducts, shortening the conjugated system while saturating the 4,5-double bond (Figure S1A). This PVB formation is frequently incomplete when DXCF CBCRs are expressed in *Escherichia coli*,[31,35] and the resulting mixed populations have given rise to conflicting interpretations of the chromophore structure in the literature.[24,25,27] The recent demonstration of multiple bilin populations in the DXCF CBCR TePixJ and of the presence of an additional free thiol group in its photoproduct state[35] reconciles the earlier data and supports the DXCF photocycle model shown in Figure 1.

In this model, both PVB and PCB populations of DXCF CBCRs possess indistinguishable blue-absorbing dark states due to thiol adduct formation at C10 (Figure 1). Primary photochemistry therefore must occur at C15 because the PVB population has a saturated C5 methine bridge and C10 is saturated by thioether linkage formation. After blue light triggers *15Z*-to-*15E* isomerization, thermal cleavage of the linkage at C10 accounts for the large red-shift of the photoproduct absorbance as conjugation is restored across the C10 methine bridge (Figure 1). The PVB population absorbs green light, resulting in the familiar blue/green photocycle when PVB is in excess relative to PCB. Photoconversion of both products restores the *15Z* configuration, followed by spontaneous thermal re-formation of the second linkage to complete the photocycle. The majority PVB population is detected upon acid denaturation of the protein,[25,27,35] while the minority PCB population can be detected by circular dichroism spectroscopy[24] and by characterizing the photochemistry of the acid-denatured photoproduct state.[31,35,41]

The present study was undertaken to address several questions that remain unanswered about the DXCF CBCRs. Does PCB to PVB isomerization always occur for members of this subfamily? If not, what factors influence this isomerization? What is the spectral region spanned by this subfamily? To

dx.doi.org/10.1021/bi201783j | *Biochemistry* 2012, 51, 1449−1463

address these questions, we have performed a survey of all members of this subfamily encoded in the genome of the filamentous cyanobacterium *Nostoc punctiforme* ATCC 29133. We tested 18 possible photosensors, 15 of which have both conserved Cys residues of the DXCF subfamily. This survey yielded 14 photoactive proteins. These newly characterized CBCRs provide valuable insights into the spectral diversity of DXCF CBCRs and into the requirements for PVB formation, demonstrating that these proteins sense a much broader range of light than previously appreciated.

MATERIALS AND METHODS

Bioinformatics. CBCR sequences were aligned with other DXCF CBCRs published to date, SyPixJg2, TePixJ, Tlr0924, and UirS (also known as Slr1212, SyETR1, and PixA)[24−27,31,41] using MUSCLE[42] followed by manual addition of AnPixJg2, NpR6012g4, SyCcaS, and NpCcaS. Manual alignment used a number of conserved residues, highlighted in Figure S2.

Cloning and Expression of CBCRs. Purified TePixJ protein was the gift of Prof. Susan Spiller (Mills College, Oakland, CA). For other proteins, appropriate primers were used to amplify regions of interest from *N. punctiforme* genomic DNA or from plasmid pBAD-0924d.[24] Specific protein regions cloned for expression are reported in Table S1. Full-length Tlr0924 was expressed and purified exactly as described.[24] NpR2903, NpR1597g1, NpF6001, NpF1883g3, NpF1883g4, NpR5113g1, NpR5313g2, NpAF142g3, NpR1060, NpF1000, NpF6362, NpF1883g1, NpF2854g4, and both GAF-alone and GAF-GGDEF Tlr0924 were expressed in a previously described intein-CBD fusion system.[43] PCR products were digested with *Nco*I and *Sma*I and cloned into pBAD-Cph1-CBD.[43] C-terminal intein-CBD fusion proteins were coexpressed with pPL-PCB, encoding biosynthetic machinery for PCB production in *E. coli* strain LMG194.[44] Coproduction of phytochromobilin (PΦB) used a published modification of this system.[45] Coexpression of PEB used LMG194 cells and plasmid pAT-PebS (gift of Rachel Kerwin, U. C. Davis), which contains the PEB synthase PebS and its associated heme oxygenase from cyanophage PSSM2[46] in pAT101.[47] Purification using chitin resin (NEB) followed a previously described procedure,[43] with final dialysis against TKKG buffer (25 mM TES-KOH pH 7.8, 100 mM KCl, 10% (v/v) glycerol).

NpF1883g2, NpF4973, NpR6125, and NpR5113g3 gave poor expression as intein-CBD fusions, so they were expressed and characterized as C-terminally His_6-tagged proteins by cloning the equivalent regions into pET28a-RcaE (gift of Drs. Yuu Hirose and Masahiko Ikeuchi, University of Tokyo) using *Nco*I and *Bam*HI sites to keep the C-terminal His_6 tag and associated sequences in-frame. Expression then used *E. coli* strain C41[DE3][48] with plasmid pKT271 for PCB synthesis,[49] and protein was purified on Talon resin (Clontech) using an imidazole gradient (30−430 mM) with final dialysis into 20 mM sodium phosphate (pH 7.5), 50 mM NaCl, 1 mM EDTA.

Purified proteins were analyzed by SDS-PAGE using standard procedures and apparatus (Bio-Rad) followed by semidry transfer to PVDF membranes, staining with amido black for visualizing total protein, and zinc blotting[50] to confirm the presence of covalently bound bilin (Figure S3A). Some proteins were concentrated using centrifugal concentrators (10 kDa cutoff, Amicon) prior to analysis. Site-directed mutagenesis was conducted using the QuikChange Kit (Stratagene) with appropriate primers in accordance with the manufacturer's directions. All constructs were verified by nucleotide sequencing.

Characterization of CBCRs. Absorbance spectra were acquired at 25 °C on a Cary 50 spectrophotometer modified for illumination from above with a 75 W xenon source and bandpass filters.[43] The pulsed-source architecture of the Cary 50 allows acquisition of spectra during illumination, permitting better resolution of unstable photoproducts exhibiting rapid dark reversion. Rapid dark reversion was not observed for the proteins described in this study. Bandpass filters used for triggering photochemistry were 670 nm center/40 nm width (fwhm), 650 nm/40 nm, 600 nm/40 nm, 550 nm/70 nm, 500 nm/25 nm, and 400 nm/70 nm. Denaturation assays used 1:6 dilution with 6 M guanidinium chloride/100 mM citric acid, pH 2.2.[51] All proteins successfully expressed and purified in this study exhibited detectable photoconversion in the denaturation assay, indicating the presence of stable photoproducts. Native and denatured peak wavelengths are reported in Table 1, while native and denatured specific absorbance ratios (ratio of the peak chromophore absorbance on the band of longest wavelength to the peak protein absorbance of the aromatic amino acid band at 280 nm) are reported in Table 2. All photochemical difference spectra are reported as (*15Z* − *15E*).

Table 1. Peak Wavelengths of DXCF CBCRs[a]

protein	bilin	native *15Z* (nm)	native *15E* (nm)	denatured *15Z*; *15E* (nm)[b]
NpR2903	mix[c]	426	526	615 (678); 538
NpR1597g1	PVB	420	498	610; 512
NpR5113g3	PVB	422	496	604; 512
NpF6001	PCB	426	578	674; 576
NpF4973	PCB	434	602	672; 576
NpR5113g1	PVB	564	494	606; 510
NpR5313g2	PCB	550	428	672; 574
NpF1883g2	PCB	424	564	676; 574
NpF1883g2	PVB	426	500	606; 522
NpF1883g3	PCB	426	546	678; 574
NpF1883g3	PVB	424	502	608; 514
NpF1883g4	PCB	428	562	N/D
NpF1883g4	PVB	416	498	N/D
Tlr0924	PCB	436	588	674; 578
Tlr0924	PVB	436	532	609; 512
TePixJ	mix[c]	432	530	610 (655)[e]; 520
NpAF142g3[d]	mix[c]	414	414 [538]	610 (668); 526
NpR1060[d]	PCB	422	424 [?]	674; 574
NpF1000[d]	PCB	418	420 [560]	672; 584

[a]Unless otherwise noted, native peak wavelengths were calculated from photochemical difference spectra or sequential difference spectra for the transitions with the longest wavelength in each photostate. N/D, not determined. [b]Denatured peak wavelengths were calculated from sequential difference spectra or photochemical difference spectra for photoactive proteins. Values are reported for the long-wavelength transition as *15Z*; *15E* pairs. [c]Peak wavelengths are reported for the PCB/PVB mixed population. When multiple *15Z* peak wavelengths were observed, the long-wavelength value, corresponding to PCB, is reported in parentheses. [d]In cases with overlapped photoproduct and dark-state absorption, the main values were taken directly from the photoequilibrium absorption spectra. Secondary *15E* photoproducts at longer wavelengths were calculated from difference spectra and are reported in brackets. [e]Overlapping populations and protein instability complicated the analysis. Denatured wavelengths are reported for the mix, with specific PCB values in parentheses.

dx.doi.org/10.1021/bi201783j | *Biochemistry* 2012, 51, 1449−1463

Table 2. Chromophore Incorporation and C5 Saturation of CBCRs[a]

protein	bilin	reversibility (%)	native SAR	denatured SAR	PVB:PCB ratio
NpF6001	PCB	98	0.61	0.71	≪1
NpF4973	PCB	93	0.34	0.41	≪1
NpR2903	PCB/PVB	78	0.095	0.09[b]	1:1.7[c]
NpR1597g1	PVB	95	0.40	0.46	≥10:1
NpR5113g3	PVB	99	0.30	0.36	≥10:1
NpR5113g1	PVB	100	0.31	0.23	≥10:1
NpR5113g1-C_{98}A	PCB	N/D	~0.07	0.09	≪1
NpR5313g2	PCB	99	0.66	0.55	≪1
NpF1883g2	PCB/PVB	97	0.32	0.32[b]	3.2:1
NpF1883g3	PCB/PVB	93	0.42	0.54[b]	1.2:1
NpF1883g4	PCB/PVB	93	0.15	0.15[b]	1.0:1
Tlr0924	PCB/PVB	93	0.49	0.50[b]	2.9:1
NpAF142g3	PCB/PVB	58	0.21	0.23[b]	1.2:1[c]
NpR1060	PCB	91	0.45	0.44	≪1
NpF1000	PCB	64[d]	0.17	0.22	≪1

[a]Specific absorbance ratio (SAR) was calculated by dividing the peak absorbance for the bilin transition at longest wavelength by that of the protein absorbance band in the near-UV. Reversibility was calculated from forward and reverse difference spectra. Saturation ratios for mixed populations were calculated for the *15E* populations from the regenerated *15Z* spectra in sequential conversion assays unless otherwise noted. N/D, not determined. [b]Reported for the mixed population. [c]Estimated by fitting the denatured spectra as described in the Materials and Methods section. [d]The regenerated *15Z* population was spectrally distinct.

Spectral Analysis. Extinction coefficients were derived from the absorbance spectra in two steps. First, the concentration of holoprotein was estimated using published extinction coefficients for PCB (ε_{662} 35 500) and PVB (ε_{590} 38 600) under acidic denaturing conditions.[52] Second, the native absorbance spectra were corrected for holoprotein concentration using the Beer−Lambert−Bouguer law to give the native extinction coefficients reported in Table S2.

To quantitate isomerization at C5 in cases with mixed bilin populations, we evaluated four assays (Table S3). In the first assay, we assumed that the extinction coefficients of the blue bands of the blue-absorbing C10 adducts of PCB and PVB were approximately equal because the longest conjugated system of both populations is formally identical (Figure 1). Native difference spectra for each population were then calculated from sequential conversion assays (described in detail in the Results), with the ratio of the *15Z* blue-absorbing peaks representing the PVB:PCB ratio. This assay, which relies on feasibility of sequential reverse photoconversion, measures only the photochemically active *15E* population. Values from this approach are reported in Table 2 unless otherwise noted. In the second assay, aliquots denatured during sequential conversion assays were used to calculate denatured difference spectra for the individual PCB and PVB populations. Published extinction coefficients for denatured bilins (see above) were used to estimate the holoprotein concentrations for each population, from which the PVB:PCB ratio was calculated. This assay gave equivalent results to the first approach (Table S3) and also only measures the photochemically active *15E* population. In the third assay, denatured difference spectra for the two populations of NpF1883g3 obtained from sequential conversion assays were normalized with the first assay and then used to generate linear combinations for manual fitting of the denatured photochemical difference spectra for a given protein. This assay, which also measures only the active population, corroborated the results of the first two methods, thereby validating the normalization step and the first assay. In the last assay, the denatured *15Z* spectra of NpR1597g1 (PVB) and NpF6001 (PCB) were normalized using the acid-denatured extinction coefficients and used to generate linear combinations for manual fitting of the *15Z* denatured spectra. This assay allowed examination of the total population, permitting us to examine changes over days while avoiding possible complications of dark reversion; it too gave similar ratios to the others (Table S3).

***In Vitro* Assembly.** Tlr0924 and NpR5113g1 apoproteins were expressed in *E. coli* as intein-CBD fusion proteins without a second plasmid for bilin biosynthesis and were purified as for the holoprotein. Apoproteins could be stored at −80 °C for up to 6 months without loss of activity. *In vitro* assembly reactions were performed with HPLC-purified PCB[43,51] in TKKG buffer without added reductant. For assembly reactions, apoproteins were diluted in freshly prepared buffer to a concentration of 12−25 μM in a final volume of 1 mL. PCB was added from a 1 mM stock in DMSO such that the apoprotein was present in 1.2−1.3-fold excess (10−20 nmol). The presence of covalently attached chromophore following dialysis was determined by SDS-PAGE and zinc blotting as described above.

RESULTS

Defining the DXCF CBCR Subfamily in *N. punctiforme*. DXCF CBCRs contain conserved motifs around both Cys residues as well as other sequence characteristics in the first, fifth, and sixth beta strands of the GAF domain that distinguish them from the red/green[28] and green/red[30,40] CBCR subfamilies (Figure S2). To identify members of the DXCF subfamily in *N. punctiforme* (Figure 2), we used repeated BLAST[53] searches against the *N. punctiforme* genome. We identified 15 candidate domains containing both Cys residues, two domains containing only the DXCF Cys, and one other closely related domain lacking both Cys residues but still containing other sequence elements of the DXCF CBCRs (NpF1883g1[b], Figure S2). To define the functional DXCF CBCRs of *N. punctiforme,* we cloned all 18 isolated GAF domains (Table S1) as intein-CBD fusion proteins for expression in *E. coli* engineered to produce PCB.[44]

This biological relevance of this approach assumes that the recombinant proteins will be comparable to cyanobacterially

dx.doi.org/10.1021/bi201783j | *Biochemistry* 2012, 51, 1449−1463

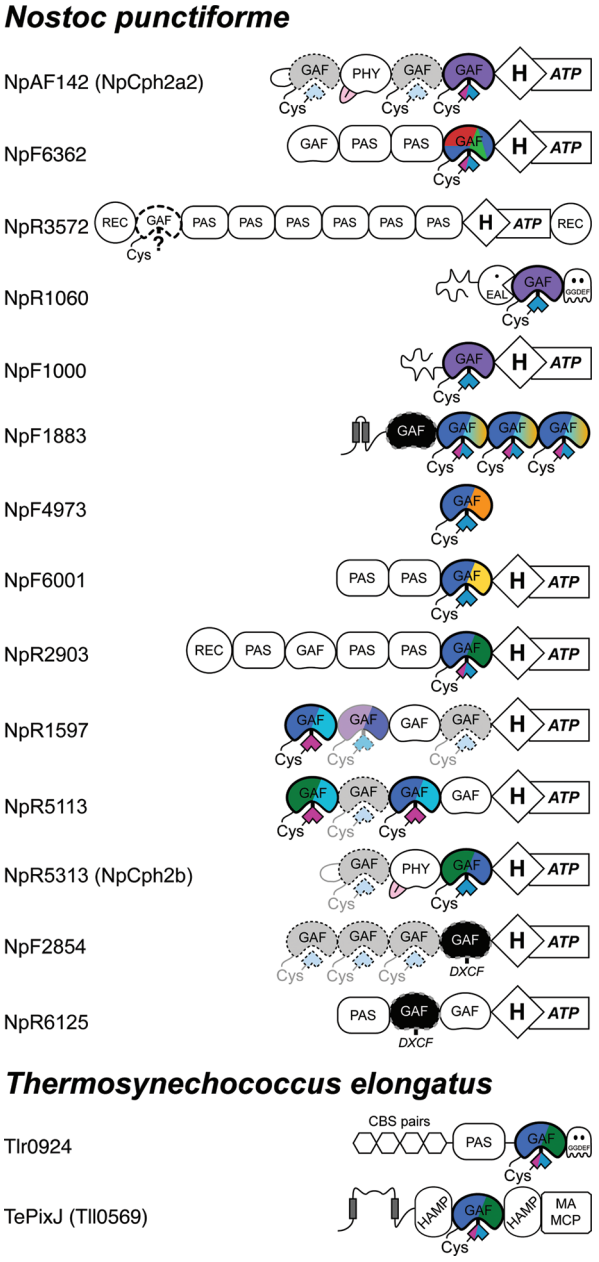

Figure 2. Domain structures of DXCF proteins in this study. Proteins from *N. punctiforme* are shown at the top, and two CBCRs from *Thermosynechococcus elongatus* also used in this study are shown at the bottom. All DXCF CBCRs examined in this study are outlined in thick black lines and color-coded by photocycle. The polygon below the GAF domain represents the bilin (blue, PCB; pink, PVB; blue/pink mix, PCB/PVB mix). NpR3572, a CBCR that failed to express, is left outlined with a "?" for the bilin. GAF domains that fail to bind bilin but that are related to DXCF CBCRs are shown in black with dashed gray outline, and undescribed CBCR GAF domains are in gray with dashed black outline. The insert-Cys CBCR NpR1597g2 (UB1[23]) is not outlined and is faintly colored. Putative transmembrane helices are shown in dark gray. REC domains, MA-MCP domains, and His kinase domains (indicated by H-ATP) are involved in two-component signaling pathways. GGDEF domains are involved in metabolism of the bacterial second messenger cyclic-di-GMP.

produced ones, that isolated GAF domains will reproduce the behavior of the same domain in full-length sensors, and that PCB is the correct chromophore precursor. Recombinant expression in *E. coli* has been shown to yield CBCRs with comparable photochemical behavior to cyanobacterially expressed proteins,[29,31,35,40] so this approach should provide accurate information about the intrinsic photochemical behavior of the isolated domains. While the effects of truncations or of possible cyanobacterial interacting proteins are harder to generalize, multiple CBCRs have been expressed as isolated GAF domains without changing their photochemical properties.[21,26,40] Moreover, we have confirmed that the photochemical properties and chromophore composition of the DXCF CBCR Tlr0924[24] are not significantly different when expressed as part of the full-length protein, as the CBCR GAF domain alone or in tandem with the adjacent GGDEF output domain (Figure S4). We therefore use the isolated Tlr0924 CBCR (designated Tlr0924 hereafter) in the present studies.

CBCRs characterized after cyanobacterial expression invariably contain PCB or PVB chromophores rather than the more oxidized bilins, phytochromobilin (PΦB) or biliverdin.[27,29,35,40] The conservation of the "first Cys" residue in CBCRs is consistent with the known A-ring thioether linkages of PCB or PΦB in plant and cyanobacterial phytochromes (Figure S2[19,54]). It is thus a reasonable assumption that CBCRs will utilize PCB as authentic chromophore precursor. While PΦB might also be expected to bind to CBCRs, as it shares the ethylidene moiety of PCB and differs only in the more oxidized 18-vinyl side chain (Figure S1A), it is not normally present in cyanobacteria. Coexpression of five DXCF CBCRs with PΦB in *E. coli*[45] all resulted in formation of stable bilin adducts (Figure S3A). One of these, Tlr0924, was also tested for its ability to incorporate phycoerythrobilin (PEB), a PCB isomer that lacks the 15,16-double bond (Figure S1A). In this case, PEB was poorly incorporated and no photochemical activity could be detected (Figure S3). Similar results were obtained with the CBCR NpF2164g3 (Figure S3), a member of the other CBCR subfamily known to use dual-Cys photocycles.[23] Taken together, these experiments indicate that the 15,16-double bond is important not only for CBCR photoconversion, as is the case in phytochromes,[55] but also for bilin binding. These pilot experiments indicate that our survey of DXCF CBCRs of *N. punctiforme* will provide insight into this photosensor subfamily.

Out of 18 targets (Figure 2), only one candidate domain, NpR3572, failed to express a stable protein (data not shown). The three proteins that lacked the first Cys (NpF1883g1, NpF2854g4, and NpR6125) all failed to bind detectable bilin (Figures S3 and S5A). Another protein, NpF6362, exhibited a blue-absorbing state with complex photochromic behavior (Figure S5B). Unfortunately, it proved thermally unstable, with rapid aggregation occurring even on ice (Figure S5C). We therefore focused on the remaining 13 proteins, which all formed stable PCB adducts (Figure S3A and data not shown). These 13 photoreceptors constitute the largest set of DXCF CBCRs characterized to date and provide valuable new insights into the flexibility of this CBCR subfamily.

DXCF CBCRs with Overlapping Photostates. Two of the DXCF CBCRs from *N. punctiforme* are found in tandem with red/far-red phytochromes of the knotless Cph2 subfamily: NpR5313g2 and NpAF142g3. One of these, NpAF142g3, exhibited a blue-absorbing dark state as expected (Figure 3A). NpR5313g2 did not and will be discussed subsequently. Illumination of the NpAF142g3 blue-absorbing dark state with violet light (400 ± 35 nm) resulted in modest bleaching and in formation of a small amount of green-absorbing photoproduct (Figure 3A and Table 1). In addition to this

dx.doi.org/10.1021/bi201783j | *Biochemistry* 2012, 51, 1449–1463

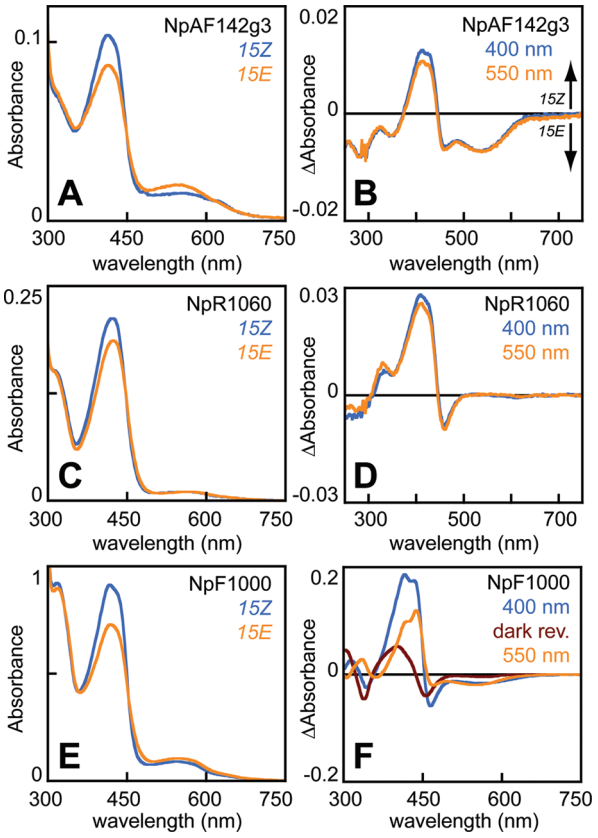

Figure 3. DXCF CBCRs exhibiting overlapped photostates. (A) Absorbance spectra of native NpAF142g3 in the *15Z* ground and *15E* photoproduct states (blue and orange, respectively). (B) Forward (blue) and reverse (orange) difference spectra of native NpAF142g3. (C) Absorbance spectra of native NpR1060, using the color scheme of panel A. (D) Forward (blue) and reverse (orange) difference spectra of native NpR1060. (E) Absorbance spectra of native NpF1000, using the color scheme of panel A. (F) Forward (blue) and reverse (orange) photochemical difference spectra and dark reversion difference spectrum (dark red) for native NpF1000. As shown in panel B, difference spectra are calculated as (*15Z* − *15E*).

photoproduct, the native photochemical difference spectrum showed negative shoulders (*15E* photoproduct) on either side of the positive *15Z* peak (Figure 3B). These shoulders raised the possibility of a second photoproduct population overlapping the dark-state absorption. Such shoulders were not seen in CBCRs with more efficient photoproduct formation (see below). Green light (550 ± 35 nm) resulted in nearly complete reverse photoconversion of NpAF142g3 (Figure 3B and Table 2). We next used the photochemistry of the acid-denatured photoproduct[35] to identify the bilin composition of NpAF142g3 (Figure S5D). As in the DXCF CBCRs TePixJ[35] and UirS,[31] two *15Z* peaks were identified at wavelengths corresponding to PCB and PVB (Figure S5E and Table 1), indicating the presence of a mixture of PCB and PVB in the photoproduct.

Two other CBCRs, NpR1060 and NpF1000, exhibited photocycles that were qualitatively similar to that of NpAF142g3. NpR1060 exhibited only a very modest bleaching of the blue-absorbing dark state and no apparent photoproduct at longer wavelengths (Figures 3C,D). Surprisingly, it was nevertheless possible to regenerate the dark state efficiently with green light (Figure 3D and Table 2). Regeneration of the dark state by green light implicates either a green-absorbing photoproduct with a very low extinction coefficient or an equilibrium between a green-absorbing state and a second photoproduct state overlapping the dark-state absorption. Denaturation analysis demonstrated the presence of only PCB in NpR1060 (Figure S5F), with the caveat that unstable species would not be detected in this assay. NpF1000 also exhibited modest loss of the dark state absorbance with formation of only a trace amount of green-absorbing photoproduct (Figures 3E,F). However, photoconversion proved surprisingly efficient, as denatured photoproduct spectra were comparable to those of the red/far-red phytochrome Cph1 (Figures S5G and S5H). This result was again consistent with either low photoproduct extinction coefficient or overlapping dark-state and photoproduct absorption. Like NpR1060, only PCB was present in NpF1000 (Figure S5I). For NpF1000, significant thermal relaxation of the photoproduct (dark reversion) was observed. Interestingly, the difference spectrum for dark reversion was distinct from that of the forward reaction in that it failed to show depletion of the green-absorbing population (Figure 3F). Reverse photoconversion of the residual photoproduct after dark reversion could be driven by green light, yet the difference spectrum was distinct from both forward photoconversion and dark reversion (Figure 3F). These data indicate that NpF1000 exhibits heterogeneity in both photostates. Moreover, the dark reversion of NpF1000 confirms the presence of a blue-absorbing *15E* population because *15Z* chromophore is regenerated during dark reversion without loss of the green-absorbing photoproduct (Figure 3F). A similar explanation likely accounts for the behavior of NpAF142g3 and NpR1060.

PVB Formation Is a Mechanism for Photoproduct Tuning. Examination of other *N. punctiforme* DXCF CBCRs revealed an awesome diversity of photocycles. Surprisingly, only NpR2903 exhibited the blue/green photocycle (Figure 4A) and a mixture of PCB and PVB (Figure 4B) previously described for TePixJ[35] and UirS/Slr1212.[31,41] NpR5113g3 and NpR1597g1 also possessed the expected blue-absorbing dark state (Figures 4C,D); however, photoconversion gave rise to a narrow photoproduct peak at 490−500 nm, in the teal[a] region of the visible spectrum. The spectrum of this photoproduct was similar to those of the α-phycoerythrocyanin (α-PEC) photoproduct[56,57] and of phycourobilin.[52,58] The extinction coefficients of these teal-absorbing photoproducts could also be much higher than those for other states (Table S2), again reminiscent of the higher extinction coefficient of phycourobilin.[52] Denaturation analysis did not show the presence of phycourobilin in these proteins (Figure 4), although the possibility of a labile "urobilinoid" adduct cannot be dismissed. Still other DXCF CBCRs yielded red-shifted photoproducts. For example, both NpF6001 and NpF4973 exhibited blue-absorbing dark states, but illumination yielded photoproducts that absorbed yellow to orange light (Figures 4E,F). Analysis of the photochemistry of denatured photoproducts revealed a primary reason for this photoproduct diversity: NpR2903 uses a mix of PCB and PVB, NpR5113g3 and NpR1597g1 use only PVB, and NpF6001 and NpF4973 use only PCB (Figure 4B and Table 1). These results thus indicate that the teal-absorbing photoproduct state of NpR1597g1 and NpR5113g3 is either a blue-shifted *15E* PVB or a labile species that collapses to *15E* PVB upon denaturation. The five CBCRs described in this section all share blue-absorbing dark states yet have distinct photoproduct states (Figure 4), revealing that the extent to

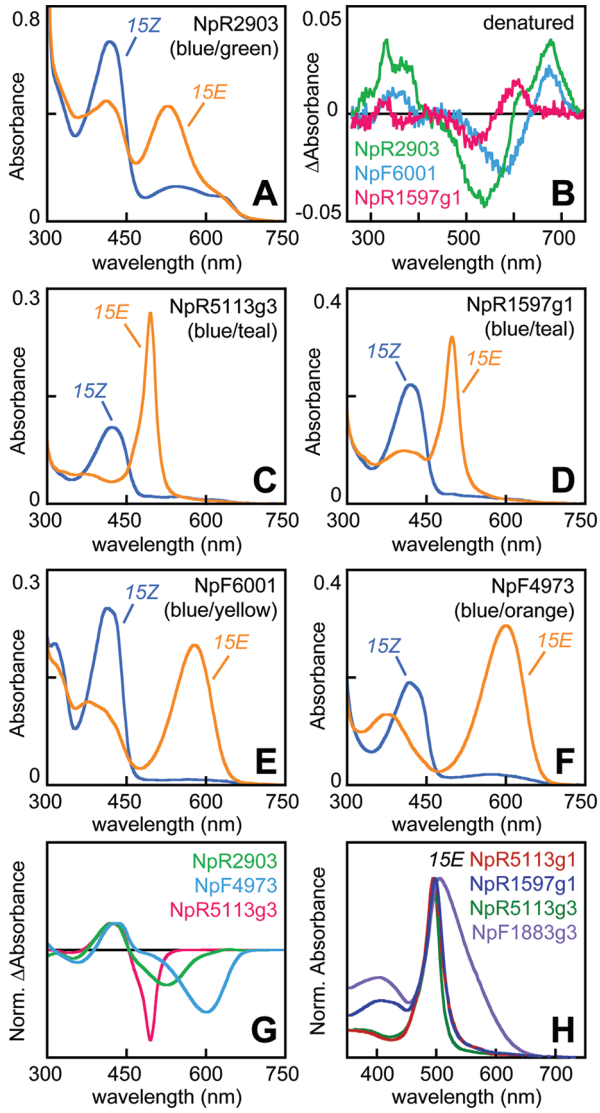

Figure 4. PVB formation allows spectral tuning of DXCF CBCRs. (A) Absorbance spectra are shown for native NpR2903 in the *15Z* ground and *15E* photoproduct states (blue and orange, respectively). (B) Photochemical difference spectra are shown for denatured *15E* NpR2903 (green, PCB/PVB mix), NpF6001 (blue, PCB chromophore), and NpR1597g1 (pink, PVB chromophore). (C) Native absorbance spectra are shown for NpR5113g3, using the color coding of panel A. (D) Equivalent spectra are shown for native NpR1597g1. (E) Equivalent spectra are shown for native NpF6001. (F) Equivalent spectra are shown for native NpF4973. (G) Photochemical difference spectra are shown for native NpR2903 (green), NpF4973 (blue), and NpR5113g3 (pink). (H) Normalized absorbance spectra are shown for the teal-absorbing *15E* photoproduct states of NpR5113g1 (red), NpR1597g1 (blue), NpR5113g3 (green), and NpF1883g3 (violet). Difference spectra are reported as (*15Z* − *15E*).

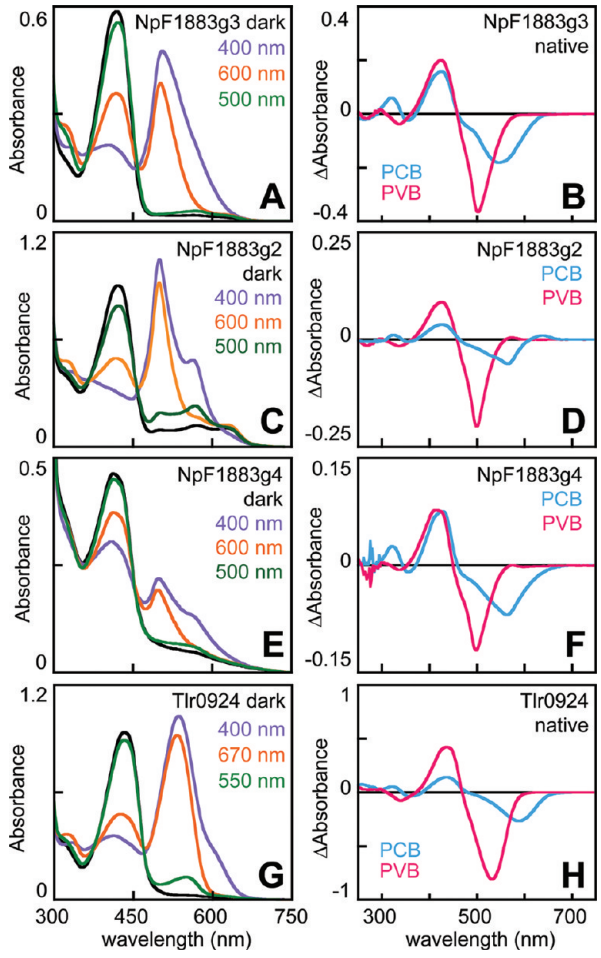

Figure 5. Sequential photoconversion of DXCF CBCRs with PCB/PVB mixes. (A) Absorbance spectra are shown for native NpF1883g3 in the dark-adapted *15Z* dark state (black) and after violet illumination (400 ± 35 nm, purple), subsequent orange illumination (600 ± 20 nm, orange), and final teal illumination (500 ± 20 nm, green). (B) Native difference spectra are shown for the reverse photoconversion of the PCB population (400−600 nm, blue) and PVB population (600−500 nm, pink) of NpF1883g3. (C) Absorbance spectra are shown for native NpF1883g2 in the same sequence as panel A. (D) Difference spectra are shown for the native PCB and PVB populations of NpF1883g2, using the approach and color scheme of panel B. (E) Absorbance spectra are shown for native NpF1883g4 in the same sequence as panel A. (F) Difference spectra are shown for the native PCB and PVB populations of NpF1883g4, using the approach and color scheme of panel B. (G) Absorbance spectra are shown for Tlr0924 in the *15Z* dark state (black), after violet illumination (purple), red illumination (670 ± 20 nm, orange), and final green illumination (550 ± 35 nm, green). (H) Native difference spectra are shown for the reverse photoconversion of the PCB population (400−670 nm, blue) and PVB population (670−550 nm, pink) of Tlr0924. Difference spectra are reported as (*15Z* − *15E*).

which individual CBCRs form PVB or retain PCB is a powerful mechanism for photoproduct spectral tuning.

Photochemically Separable PCB and PVB Populations in Native DXCF CBCRs. In addition to NpF1883g1, which does not bind bilin, the protein encoded by the *NpF1883* locus contains three DXCF CBCRs (Figure 2). All three of these proteins had blue-absorbing dark states that photoconverted under violet light (400 ± 35 nm) to give teal-absorbing product states with pronounced long-wavelength shoulders (Figure 5). Such shoulders were not seen in other teal-absorbing cases (Figure 4H). Denaturation analysis revealed that all three proteins contained mixed bilin populations (Figure S6A and Table 1), again in contrast to the other teal cases.

We therefore considered the possibility that the long-wavelength shoulders in these three domains might represent the PCB component of the photoproduct population. Illumination of the long-wavelength edge of the photoproduct absorbance in NpF1883g3 with orange light (600 ± 20 nm) resulted in specific depletion of the shoulder and regeneration of a blue-absorbing state (Figure 5A and Figure S6B).

dx.doi.org/10.1021/bi201783j | *Biochemistry* 2012, 51, 1449−1463

Photochemical analysis under denaturing conditions after illumination with 600 nm light revealed that the photoproduct obtained upon orange illumination no longer contained *15E* PCB and that only *15E* PVB remained (Figure S6A). Moreover, a sequential difference spectrum calculated from aliquots denatured after 400 nm and then 600 nm illumination proved equivalent to a denatured photochemical difference spectrum for PCB (Figure S6C). Subsequent illumination of the 600 nm photoproduct with teal light (500 ± 20 nm) resulted in depletion of residual photoproduct and regeneration of additional blue-absorbing dark state (Figure 5A). The difference spectrum calculated from denatured 600 and 500 nm photoproduct spectra was consistent with photoconversion of PVB, not PCB (Figure S6C). These studies show that orange light specifically photoconverted *15E* PCB to *15Z* PCB in the native protein with little to no photoconversion of the *15E* PVB population. Subsequent irradiation with teal light effected photoconversion of the *15E* PVB population to *15Z*. This sequential reverse photoconversion permitted calculation of difference spectra for both native PCB and PVB populations (Figure 5B), revealing the presence of nearly identical *15Z* blue-absorbing dark states for the two bilin populations.

A similar approach was used for the other two CBCR domains from the *NpF1883* locus. In NpF1883g2, the PCB population was nearly resolved as a separate peak in the 400 nm photoproduct spectrum (Figure 5C). Sequential conversion again gave PCB and PVB populations with similar dark-state absorption (Figure 5D). NpF1883g4 was less efficient at chromophore incorporation (Table 2), but the sequential conversion assay was still effective (Figure 5E). Similar dark-state absorption spectra were again seen with the two bilins (Figure 5F), albeit with a slight red shift for the PCB population (Table 1). The PVB photoproducts of all three proteins were spectrally similar, while the PCB photoproducts exhibited slight differences in line shape (Figure 5).

The ability to resolve native PCB and PVB populations by sequential conversion prompted us to reexamine Tlr0924.[24] Forward photoconversion of Tlr0924 showed heterogeneity, with appearance of a long-wavelength photoproduct at later times (Figure S6D). Moreover, illumination of the long-wavelength edge of the photoproduct mixture with red light (670 ± 20 nm) resulted in partial, wavelength-specific depletion of the photoproduct band (Figure S6E). Sequential denatured difference spectra confirmed specific photoconversion of *15E* PCB by 670 nm light (Figure S6F), and photochemical difference spectra obtained with samples denatured after 400 nm and then 670 nm light confirmed the depletion of *15E* PCB by red light (Figure S6G). It was thus possible to utilize the sequential conversion assay on Tlr0924 (Figure 5G). The blue-absorbing *15Z* transitions of both bilin populations were similar, while the PCB photoproduct displayed the expected red-shift relative to the PVB population (Figure 5H).

Interestingly, not all DXCF CBCRs with mixed bilin populations were amenable to sequential conversion. Reverse photoconversion of NpR2903 with green (550 ± 35 nm) or orange (600 ± 20 nm) light did not selectively convert the PCB population (Figure S6H and data not shown). Teal illumination (500 ± 20 nm) gave specific conversion of the PVB population at short times (Figure S6H), but longer times resulted in loss of selectivity before completion. Similarly, sequential reverse photoconversion of TePixJ failed: red light (670 ± 20 nm) did not cause photoconversion, while orange light resulted in rapid conversion of both the main population and the long-wavelength shoulder (Figure S6I). We do not currently understand the protein−chromophore interactions that determine whether a given DXCF CBCR will allow sequential conversion or not, but it is known that the *15E* PCB population of TePixJ is less photoactive than the *15E* PVB population.[35] Proteins could fail to exhibit specific conversion of PCB on a time scale of minutes in such a case.

It is also possible that proteins which fail to exhibit sequential conversion contain a labile chromophore. If this labile bilin resolved to PCB upon denaturation but spectrally overlapped the PVB population in the native protein, then there would be no selective excitation of one chromophore population and no sequential conversion. Formation of PVB from PCB has been proposed to proceed via initial formation of a C10 thiol adduct, followed by attack at the ethylidene moiety with concerted C10 elimination and C5 saturation.[39] By contrast, PVB formation in TePixJ[35] and Tlr0924 (see below) occurs after thioether formation to both the A-ring ethylidene and the C10 methine bridge. Therefore, there must be a slightly different mechanism in the DXCF CBCRs. We propose that this mechanism involves a 3,4-unsaturated intermediate (isophycoviolobilin or iPVB: Figure S1B). In DXCF CBCRs, we envisage that both covalent linkages remain stable during isomerization, with unidentified amino acids serving as general base catalysts (Figure S1B). Acid denaturation of iPVB could give rise to PCB, but iPVB would mimic PVB in the native protein. Thus, iPVB is a candidate for such a labile chromophore. Nevertheless, it is clear that DXCF CBCRs can contain mixed bilins and that the mixture of bilins that occurs in some proteins can be detected without denaturation by the sequential conversion method. These data thus provide unequivocal evidence for the presence of photoactive PCB and PVB populations in the native protein in multiple members of the DXCF CBCR subfamily.

PVB Formation Is a Reversible Equilibrium Process. The sequential conversion assay allowed us to validate several assays for measuring the PVB:PCB ratio in these proteins (Table S3; additional details are presented in the Materials and Methods). The extent to which PVB formation occurred varied among the different proteins with mixed populations (Table 2). We also examined changes in bilin composition over time for two examples with good thermal stability, Tlr0924 and NpF1883g3. Tlr0924 displayed changes in total bilin composition when incubated in the dark (Figure 6A). Moreover, PVB formation proceeded more readily when Tlr0924 was incubated in the *15E* state than in the *15Z* state (Figure 6A). The residual *15E* population had even higher PVB content (Figure S7A), indicating that dark reversion is slower for *15E* PVB than for *15E* PCB in Tlr0924. Interestingly, the total PVB content of NpF1883g3 did not continue to climb to higher values over time. Instead, the sample incubated in the *15E* photostate rapidly reached a steady-state level, while that incubated in the *15Z* photostate decreased slowly (Figure 6B). The PCB population again exhibited faster dark reversion (Figure S7A), but this effect was less pronounced than in Tlr0924. No significant change in chromophore content occurred during this incubation (Figure S7B). Therefore, the decrease in PVB:PCB ratio in *15Z* NpF1883g3 indicates that PVB and PCB are in a reversible equilibrium that is only slowly achieved. For PVB to be in excess in the *15Z* incubation, such that PCB is regenerated, also implies that the equilibrium is shifted in the two photostates, with the *15E* photostate favoring

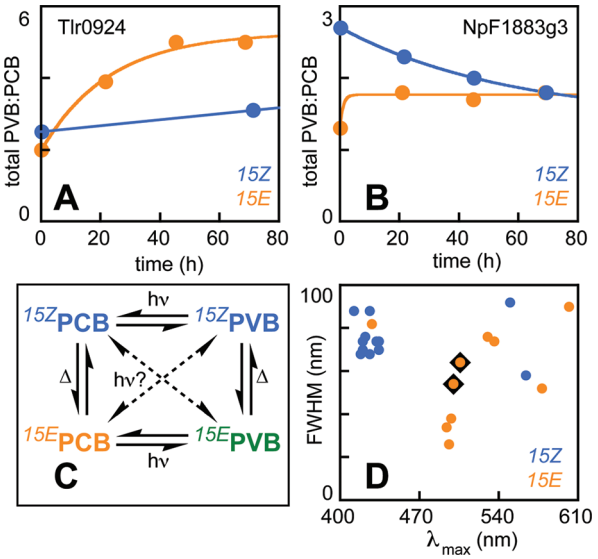

Figure 6. PVB formation is a dynamic equilibrium process. (A) Tlr0924 purified as holoprotein was incubated in darkness in the *15Z* (blue) or *15E* (orange) states for approximately 0, 22, 45, and 70 h (filled circles), and the ratio of PVB:PCB was measured by fitting the denatured *15Z* spectra as described (assay #4, Table S3). Kinetic data were fit by linear regression (*15Z*) or to a single-exponential function (*15E*). (B) NpF1883g3 purified as holoprotein was characterized as in panel A. Data from both photostates were fit to single exponential functions. (C) Thermal and photochemical equilibria inferred from panel B. (D) Full width at half-maximum bandwidth is plotted versus peak wavelength for DXCF CBCRs in which the long-wavelength transitions could be cleanly resolved from dark-state populations or other species. *15Z* transitions are in blue, *15E* transitions are in orange, and *15E* PVB populations from the *NpF1883* locus are highlighted with black diamonds.

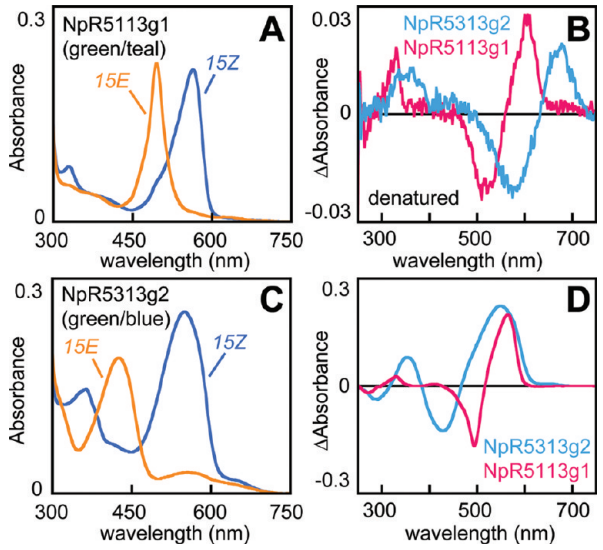

Figure 7. DXCF CBCRs with atypical dark states. (A) Absorbance spectra are shown for native NpR5113g1 in the ground (blue) and photoproduct (orange) states. (B) Photochemical difference spectra are shown for denatured NpR5313g2 (blue) and NpR5113g1 (pink). (C) Absorbance spectra are shown for native NpR5313g2, using the color scheme of panel A. (D) Photochemical difference spectra are shown for native NpR5313g2 (blue) and NpR5113g1 (pink), using the color scheme of panel B. Difference spectra are reported as (*15Z* − *15E*).

PVB relative to the *15Z* photostate (Figure 6C). In such a case, incidental formation of the *15E* photostate during expression or purification would result in formation of more PVB than would form were the protein maintained in the *15Z* photostate. Photoconversion to *15Z* would effectively create an "excess" PVB population that would equilibrate to PCB, as we have observed. The CBCR domains from the *NpF1883* locus are the only examples in which a peak absorption in the teal is not associated with an anomalously narrow line width for the absorption peak (Figure 6D). We propose that incomplete PVB formation might serve as a strategy for spectral broadening in this class of DXCF CBCRs.

DXCF CBCRs with Green-Absorbing Dark States. Two CBCRs from *N. punctiforme* did not exhibit the expected dark-state absorption in the blue to violet region of the spectrum: NpR5113g1 and NpR5313g2. NpR5113g1 exhibited a green/teal photocycle surprisingly similar to that of α-PEC (Figure 7A). The teal-absorbing photoproduct state of this protein was very similar to those of the blue/teal sensors NpR1597g1 and NpR5113g3 (Figure 4H). NpR1597g1 also displayed an additional smaller peak in the blue to violet region, implicating the presence of a stable *15E* bilin population with an intact second linkage (Figure 1), as has been proposed for Tlr0924.[24] Denaturation analysis confirmed the presence of PVB in NpR5113g1 (Figure 7B), consistent with its similarity to α-PEC.[56,57]

NpR5313g2 also exhibited a green-absorbing dark state (Figure 7C) with notable similarity to the green/red CBCR CcaS.[30,40] Like CcaS, NpR5313g2 contains PCB rather than PVB (Figure 7B). However, photoconversion of this state did not yield the red-absorbing photoproduct seen in CcaS, but a blue-absorbing photoproduct. The native photochemical difference spectrum failed to show any *15E* product in the region between 630 and 700 nm (Figure 7D), confirming that NpR5313g2 exhibits a novel green/blue photocycle. Thus, spectral tuning occurs for both *15Z* and *15E* states of DXCF CBCRs, which helps this family span a broad range between the near-UV and red regions of the visible spectrum.

Photochemical Activity Precedes PVB Formation. In TePixJ, it is known that a photoactive blue-absorbing dark state appears before any detectable PVB formation occurs.[35] Similarly, we found that Tlr0924 forms a covalently attached blue-absorbing state rapidly upon *in vitro* assembly with PCB (Figures 8A and Figure S3A). This state could reversibly photoconvert to an orange-absorbing photoproduct, and denaturation analysis detected no PVB (Figure 8B). Incubation in darkness in the *15E* state resulted in substantial PVB formation (Figure 8C), which was confirmed by sequential conversion (Figure 8D). PVB formation was much slower in the *15Z* state (Figure S7C). The native difference spectrum for the PCB population did not change over time and was almost identical to that for the PCB population in coexpressed Tlr0924 (Figure 8E). Similarly, difference spectra for the PVB populations formed during coexpression and after *in vitro* assembly showed no significant differences (Figure 8F). The PCB population has a secondary *15Z* peak at ~320 nm evident in the native PCB difference spectra but absent in the PVB difference spectra (Figures 8E,F). In the presence of the second linkage to C10 (Figure 1), the conjugated π system of the bilin is split in two. The π system associated with the A- and B-rings would be substantially blue-shifted upon PVB formation, consistent with assignment of this 320 nm band as the first electronic transition of the AB chromophore system in the PCB

dx.doi.org/10.1021/bi201783j | *Biochemistry* 2012, 51, 1449−1463

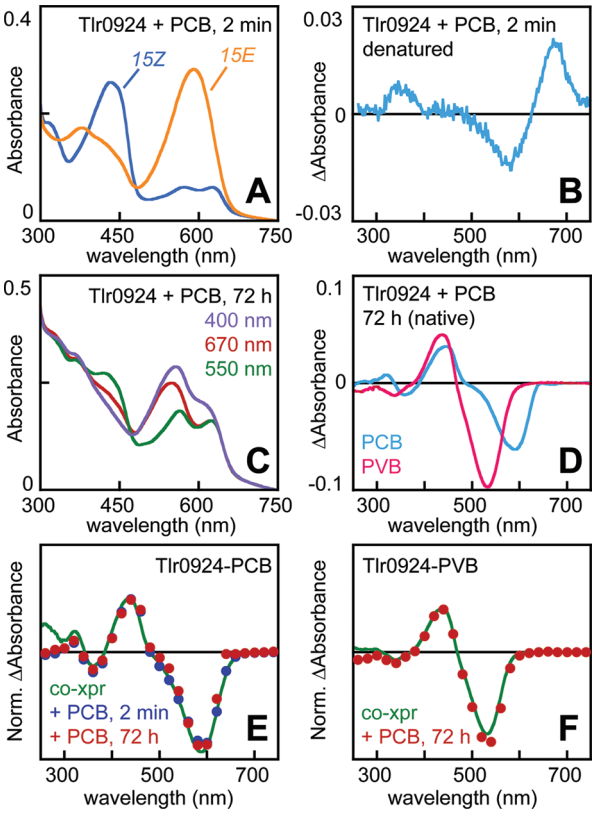

Figure 8. Photoconversion precedes PVB formation in Tlr0924. (A) Absorbance spectra are shown for Tlr0924 after *in vitro* assembly (2 min) in the *15Z* dark state (blue) and the *15E* photoproduct state (orange). (B) The denatured photochemical difference spectrum is shown for the photoproduct in panel A. (C) Sequential conversion of Tlr0924 after *in vitro* assembly with PCB, photoconversion to the *15E* state, and 72 h incubation in the dark. Spectra are shown for sequential violet, red, and green illumination (400 ± 35, 670 ± 20, and 550 ± 35 nm, respectively). (D) Native difference spectra are shown for the PCB and PVB populations from panel C. (E) Normalized native difference spectra are shown for the PCB population of Tlr0924 after coexpression with PCB biosynthetic machinery in *E. coli* (green), 2 min *in vitro* assembly (blue circles, no significant difference), and 72 h *in vitro* assembly (red circles, no significant difference). (F) Normalized native difference spectra are shown for the PVB population of Tlr0924 after coexpression (green) and 72 h *in vitro* assembly (red circles, no significant difference).

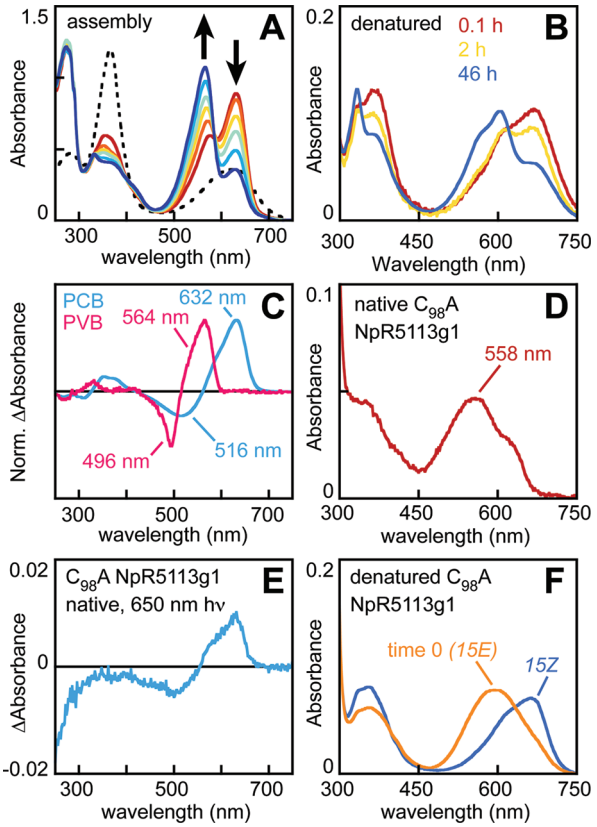

Figure 9. PVB formation requires the DXCF Cys. (A) NpR5113g1 apoprotein was assembled with PCB *in vitro* followed by incubation in the dark. Absorbance spectra show progressive conversion of PCB to PVB (time 0, red; approximately 3, 12, 24, 48, 72 h orange, yellow, light green, light blue, and dark blue, respectively). Dashed black, free PCB in the same buffer at the same concentration. (B) Absorbance spectra are shown for aliquots removed from a replicate *in vitro* assembly and denatured at the indicated times, confirming formation of *15Z* PVB. (C) Photochemical difference spectra are shown for native NpR5113g1 containing PCB (blue, 5 min. *in vitro* assembly) or PVB (pink, the same sample after overnight incubation). (D) The absorbance spectrum is shown for native C_{98}A NpR5113g1. (E) The photochemical difference spectrum is shown for native C_{98}A NpR5113g1 after illumination with red light. (F) Absorbance spectra are shown for C_{98}A NpR5113g1 immediately after denaturation (orange: predominantly *15E* PCB) and after subsequent illumination with white light (blue: *15Z* PCB). Little to no PVB could be detected.

population (Figure 1). Such an assignment would also indicate that native Tlr0924 contains PCB and not a labile 4,5-saturated species that resolves to PCB upon denaturation. These results demonstrate that Tlr0924 exhibits a robust blue-orange photocycle before any PVB is formed and implicate a photoactive PCB population retaining the 4,5-double bond.

We next used a similar approach to study PVB formation in NpR5113g1, which lacks the blue-absorbing state and instead exhibits a green/teal photocycle (see above). *In vitro* assembly of apo-NpR5113g1 with PCB resulted in rapid formation of a red-absorbing state that converted to the green-absorbing dark state over several days without accumulation of a blue-absorbing population (Figure 9A, red trace). Denaturation of aliquots taken over the course of this reaction confirmed the formation of PVB (Figure 9B). Red illumination (650 ± 20 nm) of the initial PCB adduct 5 min after addition of PCB to NpR5113g1 apoprotein resulted in photoconversion to a green-absorbing photoproduct that was red-shifted relative to the teal-absorbing PVB photoproduct observed after overnight incubation of the same sample (Figure 9C) and also observed in preparations purified as holoprotein (see above). These results demonstrate that DXCF CBCRs rapidly form photoactive PCB adducts prior to the appearance of PVB.

PVB Formation Requires the DXCF Cys Residue. In both Tlr0924 and TePixJ, mutagenesis of the DXCF Cys residue ablates formation of the blue-absorbing dark state and isomerization to PVB.[24,35] It was thus not possible to assess the role of the DXCF Cys residue in PVB formation in these proteins, as it occurs after formation of the blue-absorbing dark state. We therefore used the green/teal CBCR NpR5113g1 to address this question. C_{98}A mutant NpR5113g1 exhibited a broad, complex absorption in the red to green region of the spectrum (Figure 9D). Illumination of this species with red (650 ± 20 nm) or green (550 ± 35 nm) light resulted in only slight absorbance changes (Figure 9E and data not shown), but the difference spectra resembled those seen with the PCB

dx.doi.org/10.1021/bi201783j | *Biochemistry* 2012, 51, 1449–1463

population of wild-type NpR5113g1 (compare Figures 9C,E). Denaturation revealed the presence of substantial amounts of *15E* PCB within the mixed population (Figure 9F), with formation of little to no PVB (compare Figures 9B,F). Accumulation of *15E* PCB could either arise due to purification under green light or could indicate thermal formation of *15E* bilin, as can occur in bacteriophytochromes.[59] These data thus demonstrate that the DXCF Cys residue is required for efficient PVB formation even in the absence of a blue-absorbing dark state.

DISCUSSION

In this work, we have surveyed the complete DXCF subfamily of CBCR photosensors in *N. punctiforme*. Out of 18 total targets, only one failed to express upon recombinant expression in *E. coli* with coexpression of PCB biosynthetic machinery. Fourteen of the 17 expressed proteins contained the two conserved Cys residues of the DXCF subfamily and bound PCB, including 13 stable photoproteins. These 14 photoactive domains are derived from 11 open reading frames. Seven of the 11 putative photoreceptor genes are known to be developmentally regulated under lab conditions,[60−62] and an eighth was detected in the soluble proteome of vegetative *N. punctiforme* cells.[63] It thus seems likely that these CBCRs are part of a complex cohort of photoreceptors in this organism, implying that phenotypic analysis of photoreceptor mutants may prove complicated. Subcellular localization of these proteins will also be necessary to understand their roles in photobiology. A polar localization has been reported for at least one putative cyanobacterial photosensor.[64] Were this pattern to prove general, it would allow such proteins to carry out their photosensory functions without interference from light-harvesting pigments.

Our results confirm that the GAF domain alone is sufficient for a functional CBCR photocycle and document the versatility of this dual-Cys CBCR subfamily in spanning the visible spectrum. None of these proteins were found to contain biliverdin, which is produced as an intermediate in the biosynthesis of PCB from heme,[65] and we have shown that multiple CBCRs bind PEB only poorly. As the *N. punctiforme* genome encodes the enzymes necessary for production of biliverdin, PCB, and PEB, it is likely that PCB is the authentic chromophore precursor for these proteins and probably for the majority of CBCRs in general.

Previous examination of DXCF CBCRs has only revealed dark states ranging from the near-UV to the blue region of the electromagnetic spectrum and photoproducts in the green to yellow.[21,24−27,29,31,41] Our studies demonstrate that DXCF CBCRs exhibit astonishing diversity. We have found examples of photoproduct absorbance in the teal to orange region, green-absorbing dark states, and even a "reverse" green/blue photocycle. Our studies reveal that the ability of DXCF CBCRs to form PVB or retain PCB is a powerful means for tuning the photoproduct absorption without shifting the dark-state absorption (Figure 4G). While quite broad, the spectral coverage of DXCF CBCRs in *N. punctiforme* has a gap at ∼450 nm. This spectral gap is well complemented by insert-Cys CBCRs with photoproducts that absorb maximally in this region.[23] Dual-Cys photosensors of the phytochrome superfamily thus provide complete coverage of the visible and near-UV spectrum (Figure S8). DXCF and insert-Cys CBCRs use different strategies for spectral tuning, as insert-Cys CBCRs vary the stability of the second linkage rather than using PVB formation.[23] It is thus conceivable that various physiological signals could differentially influence the light sensing ability of one subfamily of dual-Cys CBCRs, allowing integration of the light environment with metabolic cues such as pH, redox potential, or free thiol concentration at the level of the photosensor itself.

We have characterized multiple examples of apparently inefficient photosensors with little to no apparent photoproduct formation in native samples (Figure 3). Such photocycles exhibit obvious similarity to that of SyCikA.[29] Indeed, the closest relative of SyCikA in *N. punctiforme* is NpF1000 (Figure S2). In this protein, we have demonstrated the presence of a blue-absorbing photoproduct population that strongly overlaps the dark-state absorption (Figure 3). It seems plausible that other such proteins with overlapped dark-state and photoproduct populations could have evolved via stabilization of the second linkage in the *15E* state (Figure 1). Such a model could also explain the surprising reverse photoconversion of NpR1060 with green light despite the apparent lack of a green-absorbing photoproduct (Figure 3): were a green-absorbing population to be in equilibrium with such a cryptic photoproduct, green light would slowly deplete that photoproduct and provide efficient, specific reverse photoconversion. Forward photoconversion in such cases must reflect formation of a photoequilibrium between the *15Z* and *15E* blue-absorbing photostates that favors the *15E* state. Efficient forward photoconversion in NpF1000 and NpAF142g3 (Figure S4) therefore must result from poor reverse photochemistry. Such overlapped cases can still undergo PVB formation, because NpAF142g3 contains a mix of PCB and PVB adducts (Figure S4).

Conversion of PCB into PVB requires saturation of the 4,5-double bond of PCB and desaturation of the 2,3-single bond (Figure S1A). As such, it is properly viewed as an isomerization reaction, perhaps proceeding via an iPVB intermediate (Figure S1B). PVB formation in TePixJ and UirS/PixA is complete upon expression in *Synechocystis* but incomplete upon expression in *E. coli*.[35,41] Our work shows that this isomerization is a spontaneous process that can still be incomplete after purification. We also show that this isomerization equilibrium can differ between *15Z* and *15E* states (Figure 6). Hence, the extent of PVB formation in a given protein preparation reflects both light exposure during purification and the elapsed time between induction of expression and completed purification. These results imply that cyanobacterial expression systems are much more likely to exhibit complete isomerization due to their longer growth periods in the presence of light. They further imply prep-to-prep variation for a given protein. Specific protein−chromophore interactions of individual CBCRs can also have a profound effect on the rate of PVB formation. Blue/teal cases are able to complete the reaction during expression in *E. coli*. Blue/yellow and blue/orange cases, which do not form PVB at all on the same time scale, seem likely not to do so in cyanobacteria either.

We have demonstrated that at least one DXCF CBCR, NpF1883g3, maintains a mixture of PVB and PCB in dynamic equilibrium over time (Figure 6B). As an intrinsic thermodynamic property of the protein, this is likely to hold true within the cyanobacterial cell as well, unless there are specific factors in the cyanobacterial cell that alter this equilibrium. While lyases perform such a function in assembly of phycobiliproteins, this is a different situation: phycobiliproteins are not able to incorporate bilin without lyases, and the lyase determines the

final identity of the bilin incorporated into the phycobiliprotein.[66,67] Phytochromes and CBCRs do not need such accessory proteins because they are able to self-assemble with bilin chromophores. The selective advantage conferred by maintaining a stable mixture of chromophores in a CBCR over several days is not currently clear. However, it is interesting to note that NpF1883g3 and its closest relatives have a unique combination of teal peak absorbance and broad peak width (Figures 4F and 6D). It thus is possible that maintaining a mixture of PCB and PVB populations allows a photosensor with both high sensitivity in the teal region of the spectrum and sensitivity to green or orange light. Combining such a sensor with narrower or partially overlapping responses from other CBCRs could potentially allow very fine distinctions to be made in color sensing in the green region of the spectrum, an important band for light harvesting and complementary chromatic acclimation in cyanobacteria.[68]

Our studies also provide new insights into the photocycles of DXCF CBCRs. We have confirmed that formation of the blue-absorbing dark state precedes PVB formation and have established the presence of PCB and PVB mixtures in native samples. Neither of these observations is consistent with a stable second linkage at C5, as has been proposed for TePixJ.[25] In DXCF CBCRs with photoactive PVB, photochemistry cannot occur at C5. Denaturation analysis clearly demonstrates that the primary photochemistry in such proteins is equivalent to that in α-PEC, which is photoisomerization of the 15,16-double bond (this work and refs 27, 35, 56, 57, and 69). Equivalent blue-absorbing dark states are seen with the PCB and PVB populations of the same protein (Figure 5 and Table 1), demonstrating that the C5 methine bridge is not part of the conjugated system in the blue-absorbing *15Z* state. By contrast, *15E* PCB populations are consistently red-shifted relative to *15E* PVB populations in mixed cases amenable to sequential conversion (Figure 5 and Table 1). This result indicates that the C5 methine bridge is part of the conjugated system in the *15E* photostate. These data clearly demonstrate that there is a change in the conjugation of the methine bridges upon photoconversion. This change in conjugation cannot occur at C15 (the site of primary photochemistry) or C5 (the site of PVB formation), so it must occur at C10. This implicates cleavage of a C10 adduct in the photoproduct state to yield blue/teal, blue/green, and blue/orange photocycles, as shown in Figure 1. In cases with mixed bilins, the PCB and PVB populations are capable of following parallel cycles (Figure S9), but the key point of the photocycle remains the same: light-regulated second linkage formation at C10.

This model cannot explain the anomalous green/teal and green/blue photocycles that this study has revealed (Figure 7). In NpR5113g1, the chromophore is PVB and the green/teal photocycle closely resembles that of α-PEC.[56,57] NpR5113g1 is thus likely to have a photocycle similar to that of α-PEC, with a protonated *15Z* PVB dark state and a twisted photoproduct that collapses to the *15E* state upon denaturation (Figure S10A). Such a twisted photoproduct has been confirmed crystallographically in α-PEC.[69] Despite the absence of a blue-absorbing dark state in this CBCR, the DXCF Cys is nevertheless critical for PVB formation (Figure 9). Although a blue-absorbing species does not accumulate during PVB formation in NpR5113g1, we cannot rule out the transient formation of such a species. Such a transient second linkage at C10 could facilitate isomerization to PVB (Figure S10B) in a situation analogous to that described for the reaction of PCB with thiols in solution.[39] Alternately, the DXCF Cys could serve as a general base catalyst for PVB formation. While these models remain speculative, either would explain the requirement for the DXCF Cys in PVB formation.

The other green-absorbing dark state found here is that of NpR5313g2, which uses PCB rather than PVB for its green/blue photocycle. In this case, we propose that the dark state is a deprotonated *15Z* chromophore, making it less electrophilic and explaining its blue-shift (Figure S7C). Photoconversion would generate a deprotonated *15E* primary photoproduct; were that species to become protonated, it would be more susceptible to nucleophilic attack at C10. The variant DXCF motif of this protein (Figure S2) could well shift its position slightly, favoring attachment to the *15E* photostate and resulting in the observed blue-absorbing photoproduct. Reverse photoconversion would result in a *15Z* photoproduct also absorbing in the blue. This primary photoproduct would regenerate the green-absorbing state via elimination of the DXCF Cys thiol group attached to the C10 position, followed by proton transfer.

In summary, we have found striking diversity in the wavelength sensing range of DXCF CBCRs encoded within a single organism. This diversity may explain the broad distribution of the DXCF subfamily because it provides great light-sensing versatility. Our studies also show that the particular DXCF photocycle cannot currently be predicted from primary amino acid sequence. It remains of special interest to see whether other organisms have evolutionarily selected novel dual-Cys CBCRs extending further into the near-UV or red. The discovery of the dual-Cys phytochrome TP1 demonstrates that such violet/red photocycles are possible with PCB chromophores.[23] Thioether linkage to the bilin C10 atom is clearly a powerful means of using a red-absorbing chromophore to span the entire spectrum and to combine both blue or violet and red photoperception in a single chromophore.

■ ASSOCIATED CONTENT

Supporting Information

Figures S1−S10 and Tables S1−S3. This material is available free of charge via the Internet at http://pubs.acs.org.

■ AUTHOR INFORMATION

Corresponding Author

*Tel: 530-752-1865; Fax: 530-752-3085; e-mail: jclagarias@ucdavis.edu.

Funding

This work was supported by a grant from the Chemical Sciences, Geosciences, and Biosciences Division, Office of Basic Energy Sciences, Office of Science, United States Department of Energy (DOE DE-FG02-09ER16117 to J.C.L.). Cloning of Tlr0924 was funded by a subcontract from the National Science Foundation Center for Biophotonics Science and Technology PHY-0120999 to J.C.L.

Notes

The authors declare no competing financial interest.

■ ACKNOWLEDGMENTS

We thank Dr. Yuu Hirose, Dr. Takami Ishizuka, Prof. Rei Narikawa, and Prof. Masahiko Ikeuchi (University of Tokyo) for plasmid pET28a-RcaE and for helpful discussions. We also thank Elsie L. Campbell and Prof. Jack Meeks (U. C. Davis) for

the generous gift of *N. punctiforme* genomic DNA, Prof. Susan Spiller (Mills College) for the gift of TePixJ and full-length Tlr0924, Prof. Nicole Frankenberg-Dinkel (Ruhr-University Bochum) for the cyanophage PEB biosynthesis operon, Prof. Takayuki Kohchi (Kyoto University) for the gift of plasmid pKT271, Rachel Kerwin (U. C. Davis) for the preparation of pAT-PebS during her lab rotation, and Ms. Ari Dwi Nugraheni (Nara Institute of Science and Technology) for technical assistance with the early stages of this project.

■ ABBREVIATIONS

Δabsorbance, change in absorbance (in difference spectra, which are reported as *15Z* − *15E*); α-PEC, α-phycoerythrocyanin; CBCR, cyanobacteriochrome; CBD, chitin-binding domain; DXCF, Asp-Xaa-Cys-Phe motif defining a subfamily of dual-Cys CBCRs; Et, ethyl; GAF, domain acronym derived from vertebrate cGMP-specific phosphodiesterases, cyanobacterial adenylate cyclases, and formate hydrogen lyase transcription activator FhlA; HPLC, high-performance liquid chromatography; iPVB, isophycoviolobilin, having saturated C2 and C5 carbons and a 3,4-double bond (Figure S1B); P, propionate; P_r, red-absorbing state of phytochrome; P_{fr}, far-red-absorbing state of phytochrome; PHY, domain specific to red/far-red phytochromes, C-terminal to the GAF domain; PCB, phycocyanobilin; PCR, polymerase chain reaction; PEB, phycoerythrobilin; PΦB, phytochromobilin; PVB, phycoviolobilin; PVDF, poly(vinylidene difluoride); SDS-PAGE, denaturing polyacrylamide gel electrophoresis with sodium dodecyl sulfate; TES, *N*-[tris(hydroxymethyl)methyl]-2-aminoethanesulfonic acid; TKKG buffer, 25 mM TES-KOH pH 7.8, 100 mM KCl, 10% (v/v) glycerol; Vn, vinyl.

■ ADDITIONAL NOTES

[a]Throughout, we designate photocycles by the *15Z* dark state followed by the *15E* lit state. Thus, we designate DXCF CBCRs such as TePixJ or Tlr0924 as blue/green: a blue-absorbing *15Z* dark state photoconverting to and from a green-absorbing *15E* photoproduct. Color definitions used in this study are near-UV, 300−395 nm; violet, 395−410 nm; blue, 410−480 nm; teal, 480−520 nm; green, 520−570 nm; yellow, 570−580 nm; orange, 580−615 nm; red, 615−685 nm; far-red, 685−750 nm. Given that all CBCRs are cyanobacterial proteins, we adopt the 'teal' state rather than 'cyan' state to avoid confusion.

[b]We designate the new proteins in this study by reference to the GenBank locus tag (e.g., *NpF1883)*, which is a unique designation for the open reading frame. GAF domains which contain recognizable sequence elements of the phytochrome lineage are numbered from the N-terminus. Thus, for the *NpR1597* locus, there are four GAF domains, all of which show homology to phytochromes. NpR1597g1 is the most N-terminal of these domains. For cases in which there is a single phytochrome-type GAF domain, no number is assigned (e.g., NpF4973).

■ REFERENCES

(1) Möglich, A., Yang, X., Ayers, R. A., and Moffat, K. (2010) Structure and function of plant photoreceptors. *Ann. Rev. Plant Biol. 61*, 21−47.

(2) Christie, J. M. (2007) Phototropin blue-light receptors. *Ann. Rev. Plant Biol. 58*, 21−45.

(3) Schafmeier, T., and Diernfellner, A. C. (2011) Light input and processing in the circadian clock of Neurospora. *FEBS Lett. 585*, 1467−1473.

(4) Chaves, I., Pokorny, R., Byrdin, M., Hoang, N., Ritz, T., Brettel, K., Essen, L. O., van der Horst, G. T., Batschauer, A., and Ahmad, M. (2011) The cryptochromes: blue light photoreceptors in plants and animals. *Ann. Rev. Plant Biol. 62*, 335−364.

(5) Gomelsky, M., and Hoff, W. D. (2011) Light helps bacteria make important lifestyle decisions. *Trends Microbiol. 19*, 441−448.

(6) White, D., Shropshire, W. Jr., and Stephens, K. (1980) Photocontrol of development by Stigmatella aurantiaca. *J. Bacteriol. 142*, 1023−1024.

(7) Blumenstein, A., Vienken, K., Tasler, R., Purschwitz, J., Veith, D., Frankenberg-Dinkel, N., and Fischer, R. (2005) The Aspergillus nidulans phytochrome FphA represses sexual development in red light. *Curr. Biol. 15*, 1833−1838.

(8) Giraud, E., Zappa, S., Vuillet, L., Adriano, J. M., Hannibal, L., Fardoux, J., Berthomieu, C., Bouyer, P., Pignol, D., and Vermeglio, A. (2005) A new type of bacteriophytochrome acts in tandem with a classical bacteriophytochrome to control the antennae synthesis in Rhodopseudomonas palustris. *J. Biol. Chem. 280*, 32389−32397.

(9) Sharrock, R. A. (2008) The phytochrome red/far-red photoreceptor superfamily. *Genome Biol. 9*, 230.

(10) Franklin, K. A., and Quail, P. H. (2010) Phytochrome functions in Arabidopsis development. *J. Exp. Bot. 61*, 11−24.

(11) Barkovits, K., Schubert, B., Heine, S., Scheer, M., and Frankenberg-Dinkel, N. (2011) Function of the bacteriophytochrome BphP in the RpoS/Las-quorum sensing network of Pseudomonas aeruginosa. *Microbiology 157*, 1651−1664.

(12) Rockwell, N. C., Su, Y. S., and Lagarias, J. C. (2006) Phytochrome structure and signaling mechanisms. *Annu. Rev. Plant Biol. 57*, 837−858.

(13) Rockwell, N. C., and Lagarias, J. C. (2010) A brief history of phytochromes. *ChemPhysChem 11*, 1172−1180.

(14) Auldridge, M. E., and Forest, K. T. (2011) Bacterial phytochromes: More than meets the light. *Crit. Rev. Biochem. Mol. Biol. 46*, 67−88.

(15) Wagner, J. R., Brunzelle, J. S., Forest, K. T., and Vierstra, R. D. (2005) A light-sensing knot revealed by the structure of the chromophore binding domain of phytochrome. *Nature 438*, 325−331.

(16) Yang, X., Kuk, J., and Moffat, K. (2008) Crystal structure of Pseudomonas aeruginosa bacteriophytochrome: photoconversion and signal transduction. *Proc. Natl. Acad. Sci. U. S. A. 105*, 14715−14720.

(17) Hughes, J. (2010) Phytochrome three-dimensional structures and functions. *Biochem. Soc. Trans. 38*, 710−716.

(18) Wu, S. H., and Lagarias, J. C. (2000) Defining the bilin lyase domain: Lessons from the extended phytochrome superfamily. *Biochemistry 39*, 13487−13495.

(19) Essen, L. O., Mailliet, J., and Hughes, J. (2008) The structure of a complete phytochrome sensory module in the Pr ground state. *Proc. Natl. Acad. Sci. U. S. A. 105*, 14709−14714.

(20) Essen, L. O., Anders, K., von Stetten, D., Mailliet, J., Kiontke, S., Sineshchekov, V. A., Hildebrandt, P., and Hughes, J. (2011) Spectroscopic and Photochemical Characterization of the Red-Light Sensitive Photosensory Module of Cph2 from Synechocystis PCC 6803. *Photochem. Photobiol. 87*, 160−173.

(21) Yoshihara, S., Katayama, M., Geng, X., and Ikeuchi, M. (2004) Cyanobacterial Phytochrome-like PixJ1 Holoprotein Shows Novel Reversible Photoconversion Between Blue- and Green-absorbing Forms. *Plant Cell Physiol. 45*, 1729−1737.

(22) Ikeuchi, M., and Ishizuka, T. (2008) Cyanobacteriochromes: a new superfamily of tetrapyrrole-binding photoreceptors in cyanobacteria. *Photochem. Photobiol. Sci. 7*, 1159−1167.

(23) Rockwell, N. C., Martin, S. S., Feoktistova, K., and Lagarias, J. C. (2011) Diverse two-cysteine photocycles in phytochromes and cyanobacteriochromes. *Proc. Natl. Acad. Sci. U. S. A. 108*, 11854−11859.

(24) Rockwell, N. C., Njuguna, S. L., Roberts, L., Castillo, E., Parson, V. L., Dwojak, S., Lagarias, J. C., and Spiller, S. C. (2008) A second conserved GAF domain cysteine is required for the blue/green photoreversibility of cyanobacteriochrome Tlr0924 from *Thermosynechococcus elongatus*. *Biochemistry 47*, 7304−7316.

(25) Ulijasz, A. T., Cornilescu, G., von Stetten, D., Cornilescu, C., Velazquez Escobar, F., Zhang, J., Stankey, R. J., Rivera, M., Hildebrandt, P., and Vierstra, R. D. (2009) Cyanochromes are blue/green light photoreversible photoreceptors defined by a stable double cysteine linkage to a phycoviolobilin-type chromophore. *J. Biol. Chem. 284*, 29757−29772.
(26) Yoshihara, S., Shimada, T., Matsuoka, D., Zikihara, K., Kohchi, T., and Tokutomi, S. (2006) Reconstitution of blue-green reversible photoconversion of a cyanobacterial photoreceptor, PixJ1, in phycocyanobilin-producing Escherichia coli. *Biochemistry 45*, 3775−3784.
(27) Ishizuka, T., Narikawa, R., Kohchi, T., Katayama, M., and Ikeuchi, M. (2007) Cyanobacteriochrome TePixJ of *Thermosynechococcus elongatus* harbors phycoviolobilin as a chromophore. *Plant Cell Physiol. 48*, 1385−1390.
(28) Narikawa, R., Fukushima, Y., Ishizuka, T., Itoh, S., and Ikeuchi, M. (2008) A novel photoactive GAF domain of cyanobacteriochrome AnPixJ that shows reversible green/red photoconversion. *J. Mol. Biol. 380*, 844−855.
(29) Narikawa, R., Kohchi, T., and Ikeuchi, M. (2008) Characterization of the photoactive GAF domain of the CikA homolog (SyCikA, Slr1969) of the cyanobacterium Synechocystis sp. PCC 6803. *Photochem. Photobiol. Sci. 7*, 1253−1259.
(30) Hirose, Y., Narikawa, R., Katayama, M., and Ikeuchi, M. (2010) Cyanobacteriochrome CcaS regulates phycoerythrin accumulation in Nostoc punctiforme, a group II chromatic adapter. *Proc. Natl. Acad. Sci. U. S. A. 107*, 8854−8859.
(31) Song, J. Y., Cho, H. S., Cho, J. I., Jeon, J. S., Lagarias, J. C., and Park, Y. I. (2011) Near-UV cyanobacteriochrome signaling system elicits negative phototaxis in the cyanobacterium Synechocystis sp. PCC 6803. *Proc. Natl. Acad. Sci. U. S. A. 108*, 10780−10785.
(32) Anders, K., von Stetten, D., Mailliet, J., Kiontke, S., Sineshchekov, V. A., Hildebrandt, P., Hughes, J., and Essen, L. O. (2011) Spectroscopic and photochemical characterization of the red-light sensitive photosensory module of Cph2 from Synechocystis PCC 6803. *Photochem. Photobiol. 87*, 160−173.
(33) Chen, Y., Zhang, J., Luo, J., Tu, J. M., Zeng, X. L., Xie, J., Zhou, M., Zhao, J. Q., Scheer, H., and Zhao, K. H. (2012) Photophysical diversity of two novel cyanobacteriochromes with phycocyanobilin chromophores: photochemistry and dark reversion kinetics. *FEBS J. 279*, 40−54.
(34) Nakamura, Y., Kaneko, T., Sato, S., Mimuro, M., Miyashita, H., Tsuchiya, T., Sasamoto, S., Watanabe, A., Kawashima, K., Kishida, Y., Kiyokawa, C., Kohara, M., Matsumoto, M., Matsuno, A., Nakazaki, N., Shimpo, S., Takeuchi, C., Yamada, M., and Tabata, S. (2003) Complete genome structure of Gloeobacter violaceus PCC 7421, a cyanobacterium that lacks thylakoids. *DNA Res. 10*, 137−145.
(35) Ishizuka, T., Kamiya, A., Suzuki, H., Narikawa, R., Noguchi, T., Kohchi, T., Inomata, K., and Ikeuchi, M. (2011) The Cyanobacteriochrome, TePixJ, Isomerizes Its Own Chromophore by Converting Phycocyanobilin to Phycoviolobilin. *Biochemistry 50*, 953−961.
(36) Falk, H. (1989) *The Chemistry of Linear Oligopyrroles and Bile Pigments*, Springer-Verlag, Vienna.
(37) Kufer, W., and Scheer, H. (1982) Rubins and Rubinoid Addition Products from Phycocyanin. *Z. Naturforsch. 37c*, 179−192.
(38) Chen, L. Y., Kinoshita, H., and Inomata, K. (2009) Synthesis of Doubly Locked 5Zs15Za-Biliverdin Derivatives and Their Unique Spectral Behavior. *Chem. Lett. 38*, 602−603.
(39) Tu, J. M., Zhou, M., Haessner, R., Ploscher, M., Eichacker, L., Scheer, H., and Zhao, K. H. (2009) Toward a mechanism for biliprotein lyases: revisiting nucleophilic addition to phycocyanobilin. *J. Am. Chem. Soc. 131*, 5399−5401.
(40) Hirose, Y., Shimada, T., Narikawa, R., Katayama, M., and Ikeuchi, M. (2008) Cyanobacteriochrome CcaS is the green light receptor that induces the expression of phycobilisome linker protein. *Proc. Natl. Acad. Sci. U. S. A. 105*, 9528−9533.
(41) Narikawa, R., Suzuki, F., Yoshihara, S., Higashi, S. I., Watanabe, M., and Ikeuchi, M. (2011) Novel Photosensory Two-Component System (PixA-NixB-NixC) Involved in the Regulation of Positive and Negative Phototaxis of Cyanobacterium Synechocystis sp. *Plant Cell Physiol. 52*, 2214−2224.
(42) Edgar, R. C. (2004) MUSCLE: multiple sequence alignment with high accuracy and high throughput. *Nucleic Acids Res. 32*, 1792−1797.
(43) Rockwell, N. C., Shang, L., Martin, S. S., and Lagarias, J. C. (2009) Distinct classes of red/far-red photochemistry within the phytochrome superfamily. *Proc. Natl. Acad. Sci. U. S. A. 106*, 6123−6127.
(44) Gambetta, G. A., and Lagarias, J. C. (2001) Genetic engineering of phytochrome biosynthesis in bacteria. *Proc. Natl. Acad. Sci. U. S. A. 98*, 10566−10571.
(45) Fischer, A. J., Rockwell, N. C., Jang, A. Y., Ernst, L. A., Waggoner, A. S., Duan, Y., Lei, H., and Lagarias, J. C. (2005) Multiple roles of a conserved GAF domain tyrosine residue in cyanobacterial and plant phytochromes. *Biochemistry 44*, 15203−15215.
(46) Dammeyer, T., Bagby, S. C., Sullivan, M. B., Chisholm, S. W., and Frankenberg-Dinkel, N. (2008) Efficient phage-mediated pigment biosynthesis in oceanic cyanobacteria. *Curr. Biol. 18*, 442−448.
(47) Tooley, A. J., Cai, Y. A., and Glazer, A. N. (2001) Biosynthesis of a fluorescent cyanobacterial C-phycocyanin holo-alpha subunit in a heterologous host. *Proc. Natl. Acad. Sci. U. S. A. 98*, 10560−10565.
(48) Miroux, B., and Walker, J. E. (1996) Over-production of proteins in Escherichia coli: Mutant hosts that allow synthesis of some membrane proteins and globular proteins at high levels. *J. Mol. Biol. 260*, 289−298.
(49) Mukougawa, K., Kanamoto, H., Kobayashi, T., Yokota, A., and Kohchi, T. (2006) Metabolic engineering to produce phytochromes with phytochromobilin, phycocyanobilin, or phycoerythrobilin chromophore in Escherichia coli. *FEBS Lett. 580*, 1333−1338.
(50) Berkelman, T. R., and Lagarias, J. C. (1986) Visualization of bilin-linked peptides and proteins in polyacrylamide gels. *Anal. Biochem. 156*, 194−201.
(51) Shang, L., Rockwell, N. C., Martin, S. S., and Lagarias, J. C. (2010) Biliverdin amides reveal roles for propionate side chains in bilin reductase recognition and in holophytochrome assembly and photoconversion. *Biochemistry 49*, 6070−6082.
(52) Blot, N., Wu, X. J., Thomas, J. C., Zhang, J., Garczarek, L., Bohm, S., Tu, J. M., Zhou, M., Ploscher, M., Eichacker, L., Partensky, F., Scheer, H., and Zhao, K. H. (2009) Phycourobilin in trichromatic phycocyanin from oceanic cyanobacteria is formed post-translationally by a phycoerythrobilin lyase-isomerase. *J. Biol. Chem. 284*, 9290−9298.
(53) Altschul, S. F., Madden, T. L., Schaffer, A. A., Zhang, J., Zhang, Z., Miller, W., and Lipman, D. J. (1997) Gapped BLAST and PSI-BLAST: a new generation of protein database search programs. *Nucleic Acids Res. 25*, 3389−3402.
(54) Lagarias, J. C., and Rapoport, H. (1980) Chromopeptides from phytochrome. The structure and linkage of the Pr form of the phytochrome chromophore. *J. Am. Chem. Soc. 102*, 4821−4828.
(55) Murphy, J. T., and Lagarias, J. C. (1997) The phytofluors: a new class of fluorescent protein probes. *Curr. Biol. 7*, 870−876.
(56) Zhao, K. H., Haessner, R., Cmiel, E., and Scheer, H. (1995) Type I Reversible Photochemistry of Phycoerythrocyanin Involves Z/E-Isomerization of Alpha-84 Phycoviolobilin Chromophore. *Biochim. Biophys. Acta, Bioenerg. 1228*, 235−243.
(57) Zhao, K. H., and Scheer, H. (1995) Type I and Type Ii Reversible Photochemistry of Phycoerythrocyanin Alpha-Subunit From Mastigocladus Laminosus Both Involve Z, E Isomerization of Phycoviolobilin Chromophore and Are Controlled By Sulfhydryls in Apoprotein. *Biochim. Biophys. Acta, Bioenerg. 1228*, 244−253.
(58) Killilea, S. D., and O'Carra, P. (1985) Structure and apoprotein linkages of phycourobilin. *Biochem. J. 226*, 723−731.
(59) Tasler, R., Moises, T., and Frankenberg-Dinkel, N. (2005) Biochemical and spectroscopic characterization of the bacterial phytochrome of *Pseudomonas aeruginosa*. *FEBS J. 272*, 1927−1936.
(60) Campbell, E. L., Summers, M. L., Christman, H., Martin, M. E., and Meeks, J. C. (2007) Global gene expression patterns of Nostoc punctiforme in steady-state dinitrogen-grown heterocyst-containing

cultures and at single time points during the differentiation of akinetes and hormogonia. *J. Bacteriol. 189*, 5247−5256.
(61) Campbell, E. L., Christman, H., and Meeks, J. C. (2008) DNA microarray comparisons of plant factor- and nitrogen deprivation-induced Hormogonia reveal decision-making transcriptional regulation patterns in Nostoc punctiforme. *J. Bacteriol. 190*, 7382−7391.
(62) Christman, H. D., Campbell, E. L., and Meeks, J. C. (2011) Global transcription profiles of the nitrogen stress response resulting in heterocyst or hormogonium development in Nostoc punctiforme. *J. Bacteriol. 193*, 6874−6886.
(63) Anderson, D. C., Campbell, E. L., and Meeks, J. C. (2006) A soluble 3D LC/MS/MS proteome of the filamentous cyanobacterium Nostoc punctiforme. *J. Proteome Res. 5*, 3096−3104.
(64) Kondou, Y., Mogami, N., Hoshi, F., Kutsuna, S., Nakazawa, M., Sakurai, T., Matsui, M., Kaneko, T., Tabata, S., Tanaka, I., and Manabe, K. (2002) Bipolar localization of putative photoreceptor protein for phototaxis in thermophilic cyanobacterium Synechococcus elongatus. *Plant Cell Physiol. 43*, 1585−1588.
(65) Frankenberg, N. F., and Lagarias, J. C. (2003) Biosynthesis and biological function of bilins, in *The Porphyrin Handbook. Chlorophylls and Bilins: Biosynthesis Structure and Degradation* (Kadish, K. M., Smith, K. M., and Guilard, R., Eds.) pp 211−235, Academic Press, New York.
(66) Scheer, H., and Zhao, K. H. (2008) Biliprotein maturation: the chromophore attachment. *Mol. Microbiol. 68*, 263−276.
(67) Alvey, R. M., Biswas, A., Schluchter, W. M., and Bryant, D. A. (2011) Attachment of noncognate chromophores to CpcA of Synechocystis sp. PCC 6803 and Synechococcus sp. PCC 7002 by heterologous expression in Escherichia coli. *Biochemistry 50*, 4890−4902.
(68) Kehoe, D. M., and Gutu, A. (2006) Responding to color: the regulation of complementary chromatic adaptation. *Ann. Rev. Plant Biol. 57*, 127−150.
(69) Schmidt, M., Patel, A., Zhao, Y., and Reuter, W. (2007) Structural basis for the photochemistry of alpha-phycoerythrocyanin. *Biochemistry 46*, 416−423.